NOTICE CONCERNING COPYRIGHT RESTRICTIONS

6829

Solution of Bench-Mark and Test-Case Problems Proposed by the DECOVALEX International Project

J. Noorishad and C. F. Tsang

In 1990 an international cooperative project was formed, spearheaded by the Swedish Nuclear Power Inspectorate (SKI) and Lawrence Berkeley Laboratory (LBL), for the development of coupled models and their validation against experiments in nuclear waste isolation. This project, called DECOVALEX (DEvelopment of COupled models and their VALidation against EXperiments), was initiated by a proposal to the participating organizations that a number of bench-mark tests and a test case be approved for modeling. The LBL team decided on the modeling of the bench-mark test 2 and test-case 1 problems, which will be discussed here (for details, see Noorishad and Tsang, 1992).

THE SIMULATOR

The proposed modelings involve the solution of coupled thermal-hydraulic-mechanical phenomena in the conceptualized domain of the problems. The existence of nonlinearity features requires process linearization, often in the context of an incremental loading. Large differences in the time constants of the heat flow and fluid flow problems add to the complexity of the solution scheme. LBL's ROCMAS code, developed to cope with such requirements, is used in our simulation efforts.

Bench-Mark Test 2 (BMT2)

In this problem, the subject of analysis is the thermohydromechanical behavior of a 0.5 m × 0.75 m block of hard rock intersected by four fractures. Figure 1 demonstrates the geometry and the initial and boundary conditions of the problem. The block is heated at part of the left-hand face of the block by a source with a strength of 60 W/m^2.

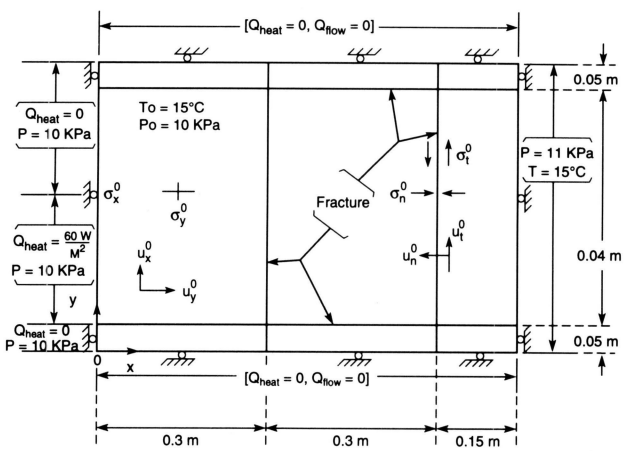

Figure 1. BMT2 model (geometry and initial and boundary conditions). [XBL 927-5735]

A linear elastic material model for the continuum and a trilinear compression and ideal elastoplastic model for the joint are used in the BMT2 model. We used two geometric discretizations for the solution. The first mesh included 252 elements and 285 nodes, and the second mesh included 1996 elements and 2091 nodes. The coarse mesh was used for the initial setup of the problem, and its very short solution turnaround time proved very useful. The refined mesh was strategically designed to reduce the truncation errors with regard to the diffusive aspects of fluid flow and heat flow. However, refinements of this order or higher cannot remedy the difficulties in solving problems that involve high Peclet and Courant numbers. Simple calculations for BMT2 showed fracture fluid velocities on the order of 10^{-2} m/sec, leading to very high grid Courant and Peclet numbers for both meshes. To overcome the expected solution difficulties of the BMT2 when flow in the fractures is considered, we employed the recent upwinding criteria suggested by Noorishad et al. (1992). The solution of the BMT2 on the refined mesh is used as the final result and as a measure of discretization sensitivity for the problem.

Solution Strategy

Another important aspect of the BMT2 solution attempt was in the selection of the solution strategy. An implicit solution of a Thermo-Hydro-Mechanical (THM) problem may require exuberant CPU times, from hours to days. However, by considering order-of-magnitude differences in the time constants of the fluid flow and heat flow evolutions, the thermal calculations (T) can be decoupled from the hydromechanical (HM) calculations. In this setup, transient calculations of the HM problem can be replaced with steady-state (snapshot) solutions at each step of the transient calculations of the heat equation. Thus the calculation load is reduced by using a fast time-marching approach to obtain the thermal solution. The solution of BMT2 began with 10^3 sec as the first time increment and was geometrically time-marched to the final total time of 10^7 sec.

Results

We obtained two alternative solutions for the BMT2. In the first solution, heat convection in the problem was neglected. The results provide a critical basis for cross-code verification. In this attempt, a maximum temperature of 21°C was obtained at the mid-point location of the source at 10^7 sec. The system was stabilized at this time as well. Figures 2 to 4 show the resulting temperatures at

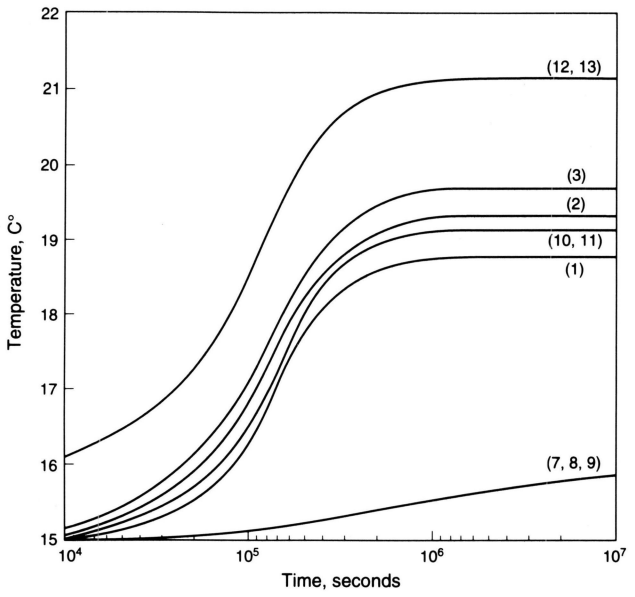

Figure 2. Temperature vs. time at various points in the mesh. [XBL 927-5744]

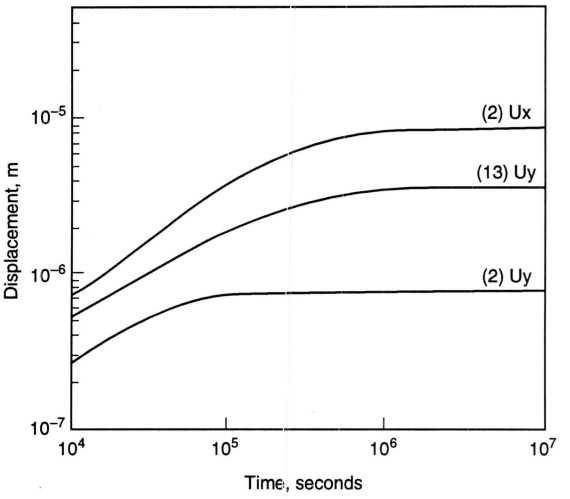

Figure 3. Displacement vs. time at various points. [XBL 927-5736]

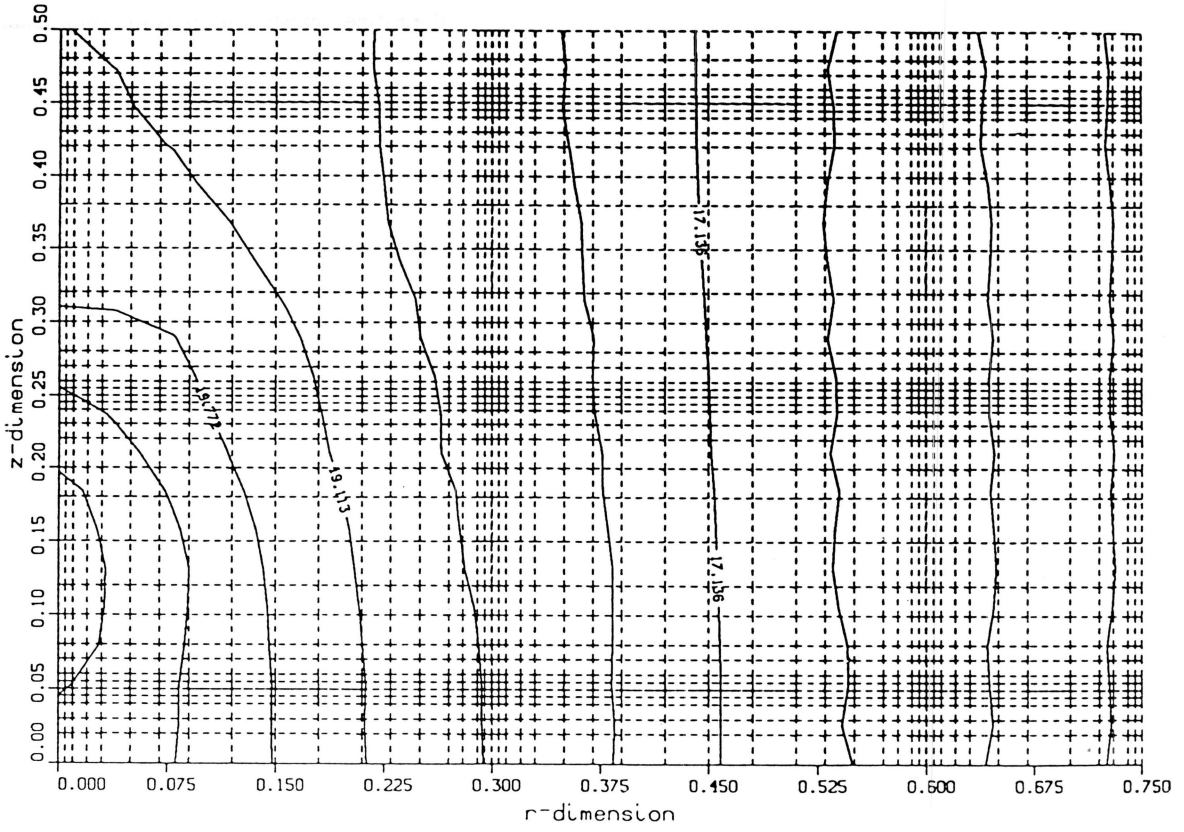

Figure 4. Temperature contours at 10^7 sec (no-convection case). [XBL 936-923]

discrete points in the mesh and provide temperature contours throughout the mesh. In the second solution, we allowed for convection in the domain. Because of the very low permeability of the continuum, fractures played the dominant role. As expected, special upstreaming (Noorishad et al., 1992) was required. With the exception of a small amount of oscillation (< 0.5°C) at 10^5 sec, the evolution of the temperature throughout the mesh was obtained as depicted in Figure 5. Comparison of the two solutions—one with and one without convection in the fractures—shows that the differences are dramatic. In the former, the cooling effect of the flow in the joints confined the heating of the rock to an area with a characteristic size almost equal to the source dimension. Using the coarse mesh, we also obtained a solution for the case with convection. Comparisons with the refined mesh results are fairly good for all of the output data.

TEST CASE 1 (TC1)

The TC1 is based on a conceptualization of the shear test in a fractured rock core, as reported in the SKB report 90-07 (Makurat et al., 1990). A fluid flow gradient is maintained during the test. Figure 6a depicts the problem configuration. Because of the low fracture fluid pressure in the test, the analysis essentially requires only mechanical simulation. However, the HM version of the ROCMAS code is utilized to do the mechanical analysis. The code also updates the fluid flow conditions in the joint as a result of the fracture closure during loading. Figure 6b shows the loading conceptualization of the test for the simulation.

Expecting various solution difficulties at the early stages of simulations of this nature, we decided to simplify the model by eliminating the steel bracket and hence the epoxy-steel contact at the boundary. Moreover, because of the complex geometry of the model, we used a nonstrategic design to generate a finite element mesh consisting of 530 four-nodal-point isoparametric elements and a total of 566 nodes. Figure 7 shows the mesh with material numbers in each element designating the epoxy (1), the rock (2), the rock joint (3), and the epoxy-epoxy contact (4). The joints are represented by a thin row of four-nodal-point joint elements that are not shown in the figure. The epoxy is assumed to be linear elastic and the epoxy-epoxy contact is a frictionless low-shear-resistant material with linear behavior in compression. The rock joint emulated a Barton-Bandis model.

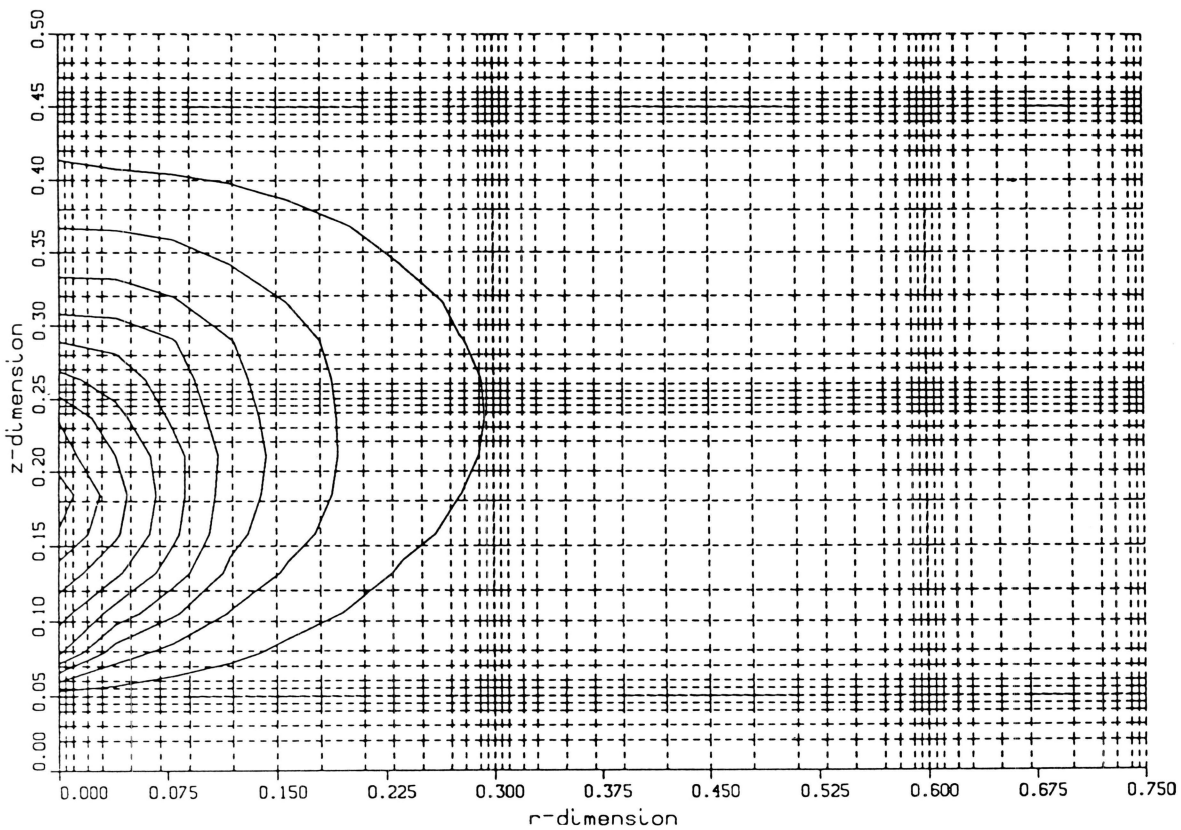

Figure 5. Temperature contours at 10^7 sec (convection case). [XBL 936-924]

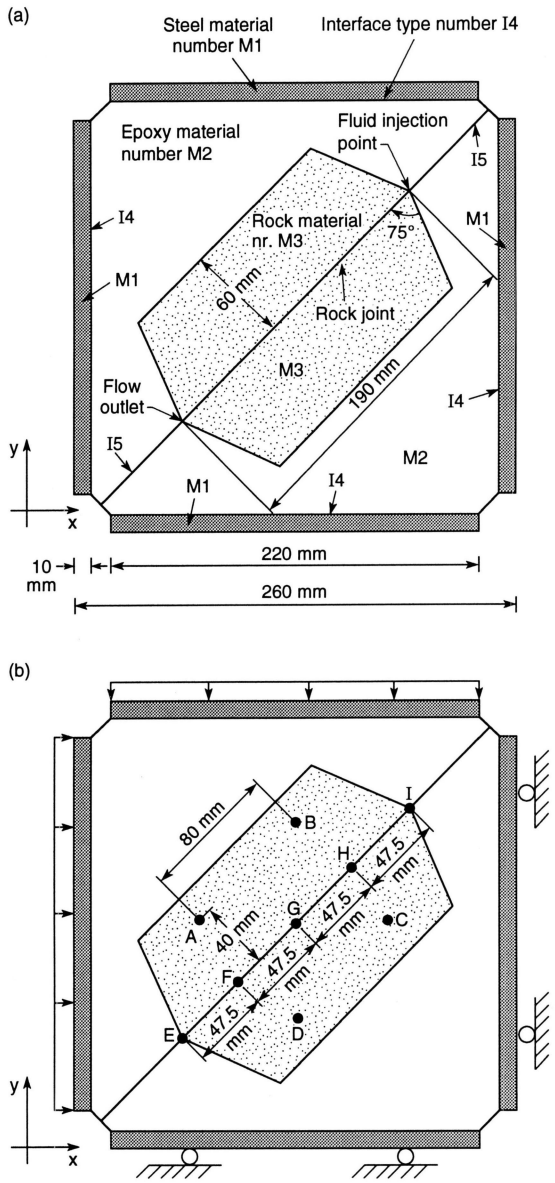

Figure 6. (**a**) TC1 model geometry and initial and boundary conditions. (**b**) TC1 loading scheme and observation points. [XBL 927-5737]

The two loading sequences—i.e., the hydrostatic loading sequence (A) and the constant displacement shear sequence (B)—were both simulated. Sequence A was performed by 5-MPa-step loading and unloading from 0 to 25 MPa and from 25 to 0 MPa. Sequence B was performed first by 5-MPa-step loading until a 25-MPa hydrostatic loading was achieved. Then, by assigning incremental displacements of +0.5, +0.3, +1.2, 2.0, –2.0, and –2.0 mm, along the fracture direction at the upper boundary (while the hydrostatic load was maintained), shearing was induced in pre- and post-failure modes at the fracture.

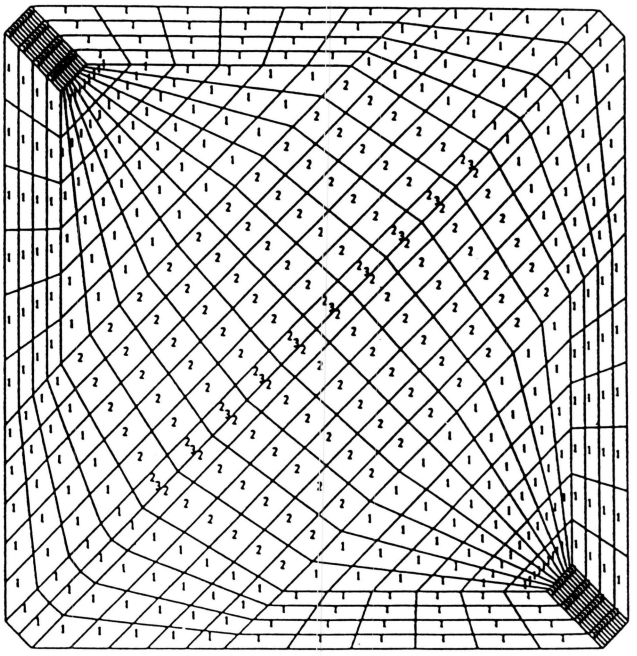

Figure 7. Finite element mesh for TC1. [XBL 936-925]

Results

Sequence A. The results of the analysis are presented in accord with the general format requested by DECOVALEX. Figure 8 shows the distribution of the average normal stress across the joint versus the average normal deformation between points A and D and B and C. As evidenced also by Figures 9 and 10, the behavior in sequence A (hydrostatic loading and unloading) is non-hysteretic, with the exception of some deviation for flow, which is expected as a result of cubic dependence on aperture.

Sequence B. The behavior in this sequence was affected markedly by two shortcomings of our model. First, the absence of the steel brackets, and hence the inability for forcing of a better distribution of the boundary loads, led to a very high concentration of stresses at the core edges. Second, this effect was further aggravated by the lack of strategic refinements of the mesh at locations on the core edges. Figure 11 demonstrates the very uneven normal stresses at the joint, which reaches a maximum at the edge. As a result, the ensuing high strength of the joint at these critical locations inhibited shear failure. The broken curve in Figure 12 exhibits the elastic behavior of the joint in forward and reverse loading.

Vivid demonstrations of the aforementioned reasons for the lack of proper performance of the model in the shear mode was attained by two small modifications of the model. In the first attempt, the epoxy was given the material property of rock while maintaining the weak epoxy-

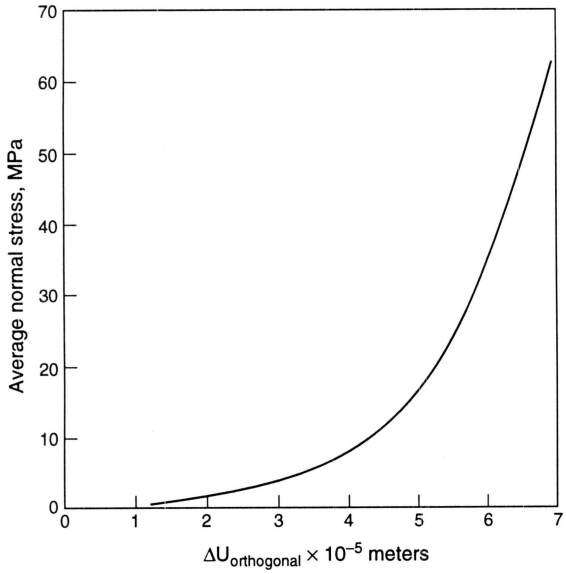

Figure 8. Average normal stress vs. average normal joint displacement. [XBL 927-5738]

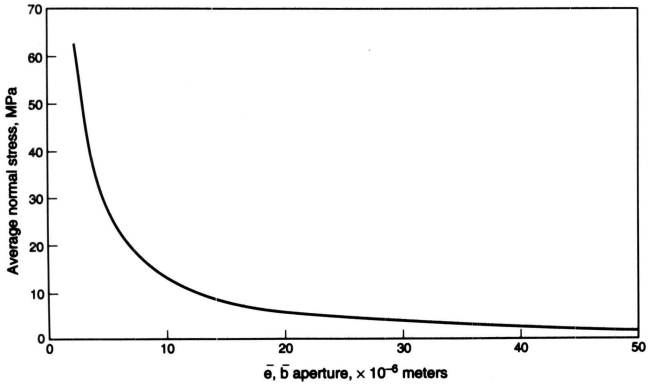

Figure 9. Average normal stress vs. average joint aperture. [XBL 927-5739]

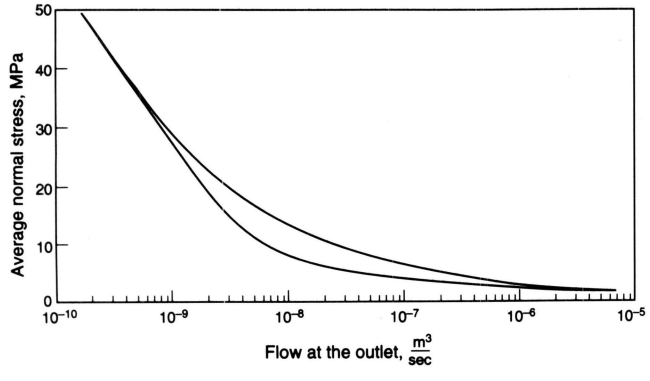

Figure 10. Average normal stress vs. outlet flow. [XBL 927-5740]

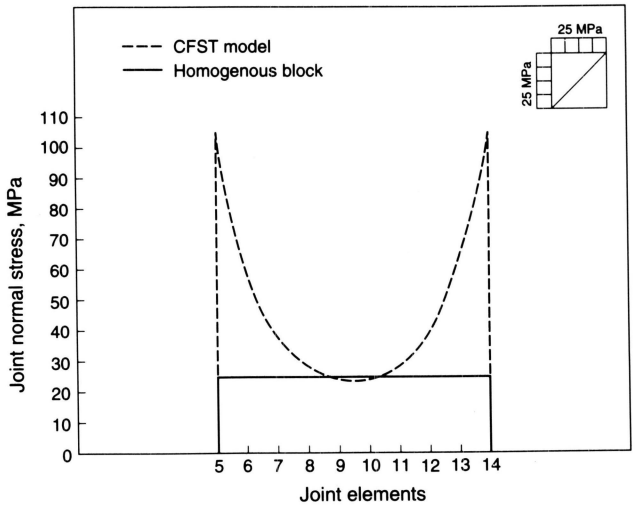

Figure 11. Joint normal stresses along the fracture. [XBL 927-5741]

epoxy contact as before. The results for this model in forward and reverse shearing are shown by the solid curve in Figure 12. The behavior is obviously more classic, with the exception of a measure of hardening caused by high stress concentration at the rock edge, where the rock joint meets the epoxy-epoxy joint. In the second attempt, the rock and the epoxy were given incompressible properties, thus eliminating the deficiencies resulting from load distribution and mesh configurations. The results of this run provide the perfect classic response shown in Figure 13.

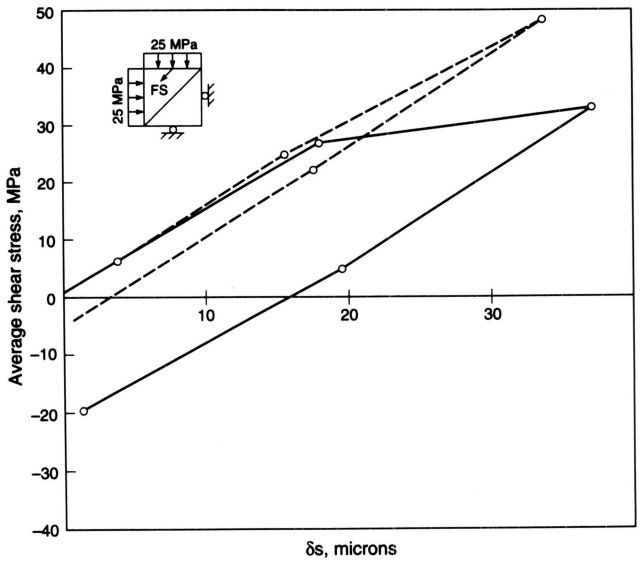

Figure 12. Average shear stress vs. average shear displacement along the joint—nonhomogeneous and homogeneous cases. [XBL 924-5745]

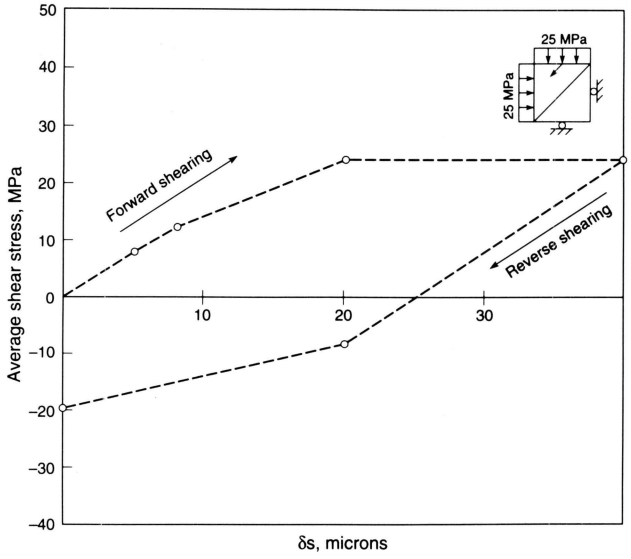

Figure 13. Average shear stress vs. average shear displacement along the joint—incompressible rock and epoxy. [XBL 924-5746]

DISCUSSION

BMT2 Problem. Because of the low strength of the heat source, only minimal HM effects on the fractures were observed. Dealing with the high-velocity heat convection proved to be the challenging part of the problem design. As a result of the cooling effects of the fracture fluid flow, heating was confined to a small part of the block. As a result, this problem served only to test the HT aspects of the THM capability.

TC1 Problem. Proper conceptualization of the test and strategically designed finite element idealization proved to be the main challenges posed by this problem. Elimination of the steel bracket from our model created very high concentrations of stress at the fracture edges. As a result, shearing became impossible. The underlying reasons became more clear when the model was altered. Prior thinking and discussion of the physics of the test should become part of the problem design for more realistic modeling.

REFERENCES

Makurat, A., Barton, N., Vik, G., and Tunbridge, L., 1990. Site characterization and validation-coupled stress-flow testing of mineralized joints of 200 mm and 1400 mm length in the laboratory and in situ, Stage 3. Swedish Nuclear Fuel and Waste Management Co., Stripa Project Report 90-07.

Noorishad, J., and Tsang, C.F., 1992. Coupled thermohydromechanical modeling bench mark Test 2 (BMT2) and Test Case 1 (TC1). DECOVALEX—Phase 1 report, 1992.

Noorishad, J., Tsang, C.F., Perrochet, P., and Musy, A., 1992. A perspective on the numerical solution of convection dominated transport problems. Water Resour. Res., v. 28, no. 2, p. 551–561.

6830

Two-Dimensional Dispersion Model for TOUGH2

C. M. Oldenburg and K. Pruess

We have added a general model for Fickian solute dispersion to the multiphase porous media transport code TOUGH2 (Pruess, 1987; 1991). Used in conjunction with the equation of state module for water, brine, and air (EOS7), the TOUGH2 Dispersion Module (T2DM) models brine transport, including the effects of molecular diffusion and hydrodynamic dispersion in rectangular two-dimensional regions. Diffusion and dispersion of vapor and air in the gas phase are also modeled. This brief report consists of a discussion of the dispersion model and its implementation in TOUGH2, followed by results from one verification problem.

FORMULATION

The general conservation equations solved by the integral finite difference method (IFDM) in TOUGH2 consist of balances between mass accumulation and flux and source terms over the grid blocks into which the flow domain has been partitioned. The flux term has contributions from both the phase flux ($\mathbf{F}_\beta$) and from dispersion and can be written

$$\mathbf{F}^{(\kappa)} = \sum_{\beta=1}^{NPH} \left(X_\beta^{(\kappa)} \mathbf{F}_\beta - \rho_\beta \overline{\mathbf{D}}_\beta^{(\kappa)} \nabla X_\beta^{(\kappa)} \right), \qquad (1)$$